Mixed-Valence Polyoxometalates: Spin-Coupling and Electron Distribution in the Decawolframate Anion Reduced by Two Electrons

Juan M. Clemente-Juan,[†,‡] Eugenio Coronado,*[,†] Alejandro Gaita-Ariño,*[†,§] and Nicolas Suaud[†,§]

Instituto de Ciencia Molecular, Universitat de Valencia, Polígono de La Coma s/n, E-46980 Paterna, Spain, Fundació General Universitat de Valencia, (FGUV), Plaça del Patriarca 4-1, 46002 Valencia, Spain, and Laboratoire de Physique Quantique, IRSAMC, Université Paul Sabatier, 118 route de Narbonne, 31062 Toulouse Cedex, France

Received: May 5, 2007

The decawolframate anion reduced by two electrons, $W_{10}O_{32}^{6-}$, is diamagnetic, and its two "extra" electrons delocalize mainly among its eight equatorial wolfram sites. In this work, we combine a phenomenological Hamiltonian with first-principles calculations to explain the origin of these properties. Through ab initio calculations and effective Hamiltonians on fragments, we determine the values of the magnetic exchange parameters, J, the transfer integrals, t, the Coulombic repulsions, V, and the orbital energies, ϵ. Then, by introducing these parameters in a model Hamiltonian simulating the whole molecule, one obtains that the singlet−triplet gap is 780 meV and that more than a 90% of the "extra" electron density resides on the eight equatorial wolfram ions. An analysis of the interplay between these parameters indicates that electron-transfer processes play a dominant role while magnetic exchange has only a minor influence.

Introduction

Polyoxometalates (POMs) constitute a rich and broad class of inorganic compounds of current interest in molecular magnetism. Besides their structural variety, they are able to accommodate various numbers of unpaired electrons, which can be either localized on a metal center or delocalized as "extra" electrons over a large number of metal centers in the so-called heteropoly blues or browns. Since the beginnings of polyoxometalate chemistry[1] to its recent advances,[2] POMs have been found to be excellent model systems to study fundamental electronic processes like magnetic exchange or electron transfer at the molecular scale.[3−5] In particular, mixed-valence POMs were studied chiefly electrochemically and optically since the sixties,[6] later by NMR and EPR,[7] and more recently are being also subject of theoretical calculations, through model Hamiltonians,[8] density functional theory,[9] and ab initio calculations.[10] Nevertheless, while some aspects of their magnetic and electrochemical properties have been clarified, we still have an insufficient comprehension of the relevant microscopic phenomena that control these properties.

Among POM, $W_{10}O_{32}^{n-}$ ($n = 4-6$), also known as decawolframate,[11] whose structure is depicted in Figure 1, is an interesting example. Long-lived complexes involving one- and two-electron reduced decawolframate participate in photocatalytic cycles such as those of electron-transfer reaction to alkenes,[12] in photodegradation of polymers and pesticides,[13] and in general in photosensitizing and photoactivation processes.[14] Thus, details of the behavior of the delocalized electrons in this structure are especially intriguing and a lot of scientific attention has arisen. This problem has already been extensively studied, both experimentally[15] and theoretically,[9,16,17] through a variety of techniques, including laser flash photolysis, vibronic theory, and density functional theory. However, to our knowledge, an exploration focusing on the magnetically relevant electronic parameters has yet to be performed. Here we present a comprehensive investigation of decawolframate with spectroscopic ab initio calculations and model Hamiltonians, with the aim of shedding some new light on this open problem.

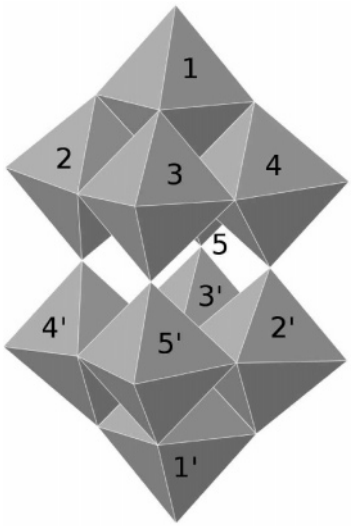

Figure 1. Structure of the $W_{10}O_{32}$ polyoxometalate and labels of the W metal ions (C_i symmetry).

In previous works, we were already able to study and rationalize the magnetic properties of some mixed-valence magnetic polyoxoanions by combining ab initio calculations on fragments to extract information about microscopic interactions with a model Hamiltonian, which is phenomenological and provides a scheme to calculate the whole system. Our initial

* Corresponding authors. E-mail: eugenio.coronado@uv.es (E.C.).
† Instituto de Ciencia Molecular, Universitat de Valencia.
‡ Fundació General Universitat de Valencia.
§ Laboratoire de Physique Quantique, IRSAMC, Université Paul Sabatier.

10.1021/jp073433y CCC: $37.00
Published on Web 09/11/2007

studies focused on the simplest case: Keggin-type anions reduced by two electrons,[10] which is a highly symmetric system. We showed that the experimentally observed diamagnetism is a consequence of the strong antiferromagnetic coupling of the two "extra" electrons arising from the combination of electron transfer and Coulombic repulsion in this type of topology and symmetry.

With the aim of exploring other topologies and symmetries, we have extended our study to the decawolframate anion reduced by two electrons, which presents the following characteristics: (i) as can be seen in Figure 1, it consists of two squares of WO_6 octahedra and two apical octahedra sharing edges or vertices and can be seen as the condensation of two monovacant Lindqvist POMs through the four oxygen vertices of the WO_6 octahedra; (ii) experimentally, it has been found to be diamagnetic and with an uneven distribution of the "extra" electrons between apical and square metals. The main difference with the Keggin structure is precisely the existence of two types of centers and three different W−O−W transfer and exchange routes.

Calculation Procedure

Model Hamiltonian of the Whole Anion. In the reduced anion, the unpaired "extra" electrons are essentially delocalized over the W d_{xy}-like orbitals (pointing in between the equatorial O ions of the octahedron). Hence, a model Hamiltonian suited to describe the magnetic properties of a reduced anion has to take into account the main effective interactions between the electrons in these orbitals. These are: the magnetic exchange interactions J_{ij}, the electron-transfer hopping integrals t_{ij}, and the electrostatic repulsions between the two electrons V_{ij}. Furthermore, the model has to take into account the energy of the "extra" electron on each metal site, ϵ. It can be written as follows:

$$H = \sum_i \epsilon_i \cdot n_i + \sum_{\langle i,j \rangle} t_{ij} \sum_\sigma (c_{i_\sigma}^\dagger c j_\sigma + c_{j_\sigma}^\dagger c_{i_\sigma}) - \sum_{\langle i,j \rangle} J_{ij} \left(\vec{S}_i \cdot \vec{S}_j - \frac{1}{4} n_i n_j \right) + \sum_{(i,j)} V_{ij} \cdot n_i n_j$$

where the sum over i runs over the d_{xy}-like orbitals of all the W centers, $\langle i,j \rangle$ runs over all nearest-neighbors W d_{xy}-like pairs, (i,j) runs over all W d_{xy}-like pairs, $\vec{S}_i$ is the local spin operator on site i, $c_{i_\sigma}^\dagger$ (respectively c_{i_σ}) are the usual creation (respectively annihilation) operators of an electron of spin σ on site i, n_i is the number operator on site i, ϵ_i is the energy of orbital i, t_{ij} is the electron transfer integral of a magnetic electron between sites i and j, J_{ij} is the magnetic exchange integral, and V_{ij} is the (intersite) electrostatic repulsion between two magnetic electrons on sites i and j. This model does not deal with configurations where two "extra" electrons are in the same orbital. Thus, it does not explicitly take into account the on-site electrostatic repulsion. In fact, the large value of the on-site electrostatic repulsion versus the intersite electrostatic repulsion does not permit those configurations to have a large weight in the low-energy wave functions. Furthermore, the model Hamiltonian does treat the effects of such configurations through the effective value of the magnetic exchange J integrals.

This model Hamiltonian is general and, if enlarged to configurations with two "extra" electrons on the same metal center if necessary (that is, when the number of "extra" electrons is larger than the number of metal centers), can be used to reproduce and understand the magnetic properties of any n-electron reduced POM.

Calculations on Embedded Fragments. The exchange, hopping, and electrostatic repulsion integrals are essentially local parameters. Therefore, they can be accurately evaluated by using ab initio spectroscopy calculations on system fragments if two conditions are met: (i) the fragment has to include all the short-range effects, which means the full coordination sphere of the magnetic atoms, and (ii) the long-range effects have to be considered, for example, by means of an appropriate bath of punctual charges. The embedded fragments calculation method fulfills these goals and its validity on mixed-valence polyoxometalates is well established and has been detailed elsewhere.[10] In this method, the model is composed by two parts: (i) a fragment based on interacting metal centers and all the atoms of their coordination sphere, (ii) an embedding of punctual charges and total-ion-pseudopotentials (TIPs). In the fragment, the interactions between the atoms are explicitly taken into account by using nuclei, electrons, large atomic basis sets, and sophisticated ab initio calculations. The aim of the embedding is to reproduce the main effects of the rest of the crystal onto the fragment, that is, the Madelung field and the Pauli exclusion. The Madelung field is modeled by a very large ensemble of suited punctual charges at the position of the ions surrounding the fragment. TIPs, encapsulating the punctual charges of the first and second shell around the fragment, reproduce the Pauli exclusion, avoiding an excessive polarization of the electrons of the fragment toward positive charges. Note that the treatment of the embedding is almost computationally costless.

The structure of a mixture of one- and two-electron reduced decawolframate has been resolved by X-ray crystallography,[18] and small differences were found for the W−O distances and W−O−W angles between this structure and the fully oxidized one (formula $W_{10}O_{32}^{4-}$). The pure two-electron reduced decawolframate structure has not, to our knowledge, been experimentally resolved, but it has been theoretically derived and was found to present very small variations from $W_{10}O_{32}^{4-}$.[17] Thus, in this work, we chose the crystallographic structure of the first historically well-resolved oxidized system, a tributylammonium salt.

This structure presents only inversion symmetry with respect to the center of the decawolframate anion, whereas the "ideal" structure (the most symmetric one) would be D_{4h}. Thus, the studied compound presents five nonequivalent W atoms and 10 nonequivalent nearest-neighbor pairs compared to two nonequivalent W atoms and three nonequivalent nearest-neighbor pairs in the "ideal" structure. Figure 1 shows the labeling of each WO_6 octahedron (1 and 1′ are symmetrically equivalent, as 2 and 2′, 3 and 3′, 4 and 4′, and 5 and 5′) and Figure 2 emphasizes the nearest-neighbor WO_6 octahedra pairs **a**, **b**, and **c**.

All types of dimeric fragments are presented in Figure 2. Because of the low symmetry of the molecule, which only bears an inversion center, there are up to 10 slightly unequal nearest-neighbor fragments, which can be grouped in three types: (1) type **a** apex-square: W(1)−W(2), W(1)−W(3), W(1)−W(4), and W(1)−W(5); (2) type **b** intrasquare: W(2)−W(3), W(3)−W(4), W(4)−W(5), and W(2)−W(5); (3) type **c** intersquares: W(2)−W(4′) and W(3)−W(5′).

Types **a** and **b** are "edge-sharing" fragments, and therefore expected to be very similar magnetochemically, and dissimilar to type **c**, which are "corner-sharing" fragments. All fragments of types **a**, **b**, and **c** were used for the determination of electron transfer t and magnetic exchange J. Besides, calculations were done on all other possible pairs (types **d**−**h** in Figure 2), including next-nearest neighbors and long-range fragments, to

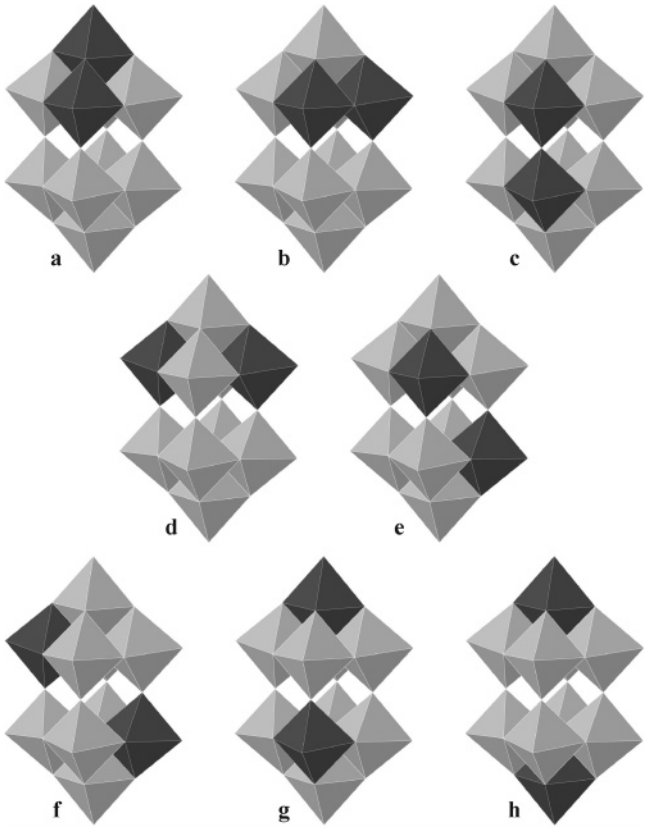

Figure 2. The 25 embedded fragments of decawolframate in C_i symmetry, at growing distance: 10 nearest-neighbors (4 **a**, 4 **b**, 2 **c**), six next-nearest neighbors (2 **d**, 4 **e**), and nine long-distance (4 **f**, 4 **g**, 1 **h**). Types **a** and **b** are W_2O_{10}, types **c** and **d** are W_2O_{11}, types **e**−**h** are W_2O_{12}.

determine all Coulombic repulsion parameters *V*. To check the consistency of the results with the size of the fragment used to extract the microscopic parameters, some trimeric fragments (not shown), containing three contiguous octahedra (type "**ab**"), were used. Comparisons between the results of calculation on dimers and on trimers are given in section "Validity of the microscopic parameters".

In Figure 3a, one can appreciate how the embedding used in the present calculations encloses the central polyoxoanion containing the fragments. It contains 27 complete $W_{10}O_{32}$ polyanions, including the central one from where the fragment is cut, each of them with its closest four surrounding countercations (not represented). This embedding is large enough to reproduce the effect of the Madelung field in the parameters under study, as determined and discussed in refs 10,19.

Figure 3b depicts the nitrogen atoms and the oxo ions closest to them, i.e., the bridging ligand between W(1) and W(4), and the apical ligand of W(5). As the hydrogen atoms are not resolved, we chose to use the positions of the nitrogens as effective location of the positive ammonium charges throughout the embedding.

Results and Discussion

The first part of this section is dedicated to check the validity of the procedure used to extract the ab initio parameters. Comparison between fragments (dimers and trimers with one or two "extra" electrons) and between methods (CASCI and DDCI) are illustrated on some examples. As a result, a set of microscopic parameter values that can reasonably be assumed to reproduce the real ones is given in Tables 3, 4, and 5 and is discussed. Then, we present an attempt to rationalize these results from structural (angles and distances) considerations.

Validity of the Microscopic Parameters. Table 1 presents, at the same level of calculation (CASCI), the values of some parameters that are extracted both from calculations on dimers ("2W") and on trimers ("3W"), with either one ("1e") or two ("2e") "extra" electrons. Transfer parameter values are almost the same in 1e−/2W and 1e−/3W calculations, proving the very good accuracy of dimer calculations and validating the choice of punctual charges and TIPs used in the bath. Comparisons with the evaluation of *t* from 2e−/3W calculations shows the influence on the electron transfer (about 100 meV) of the presence of another "extra" electron in the neighborhood of a given electron. The result is consistent with the rationalization of the origin of these effects done by Calzado and Malrieu for cuprate compounds.[29] Nevertheless, as shown later on, the electrons remain far away from one another and 1e−/2W calculations give adequate values for *t*. Similarly, *J* and *V* values extracted from 2e−/2W or 2e−/3W calculations are in good agreement, showing the order of accuracy that can be expected from 2e−/2W. More interesting is the comparison of the ϵ values with the size of the fragment as, to our knowledge, this parameter has never been extracted from CI calculations. $\epsilon_3 - \epsilon_1$ and $\epsilon_4 - \epsilon_1$ values are not so much affected by the size of the fragment. The worst estimation is for $\epsilon_2 - \epsilon_1$, the value obtained from dimer calculations is about 20% smaller than that from trimer calculations. Thus, dimer calculation evaluations of the microscopic parameters suffice for evaluating the influence of dynamical correlation mecanisms on these parameters.

Table 2 presents the evaluations from calculations on the same two dimers of *t*, *J*, ϵ, and *V* parameters at the CASCI and DDCI level of calculations. MONO and DDCI2 calculations were also performed. MONO, DDCI2, and DDCI are CI calculations based on an increasing number of dynamical correlation mechanisms. MONO and DDCI2 results are not included, as they are less accurate than DDCI and do not give any unexpected results. As usual, dynamical correlation does not play an important role for the electron transfer, whereas it is crucial for a good evaluation of *J*. In fact, this value is about 4 times stronger at the DDCI level than at the CASCI level. More interesting is to note the influence of dynamical correlation on orbital energy differences, which are almost zero for $\epsilon_3 - \epsilon_1$ and $\epsilon_4 - \epsilon_1$. Once again, the largest influence is observed on $\epsilon_2 - \epsilon_1$, which is about 20% smaller at the DDCI level. Even if this last point should be rationalized, as checked in this section, all the microscopic parameters presented in the next subsection suffice to interpret and predict the collective behavior of the two "extra" electrons delocalized over the $W_{10}O_{32}$ anion.

A Complete Set of Microscopic Parameters. Different kinds of dimers were used for extracting the values presented in Table 3 (*t* and *J*), Table 4 (ϵ), and Table 5 (*V*).

The magnetic exchange *J* is antiferromagnetic for all considered fragments. This was both expected from structural data (W−O−W angles larger than 110°) and coherent with previous results on another POM (a Keggin anion). The magnetic exchange is heavily dependent on the type of interaction: the weakest value, of the order of −120 meV, is $J_{\mathbf{a}}$, along the edge of the pyramid. It raises to the order of −250 meV inside the base of the square pyramid, i.e., fragments type **b**. Finally, the strongest magnetic exchange (about −400 meV) is $J_{\mathbf{c}}$, between the squares.

As expected, there is a parallel evolution of the values of electron transfer *t*: the smallest values (around −400 meV) are to be found for type **a** fragments, increasing to −550 meV in $t_{\mathbf{b}}$

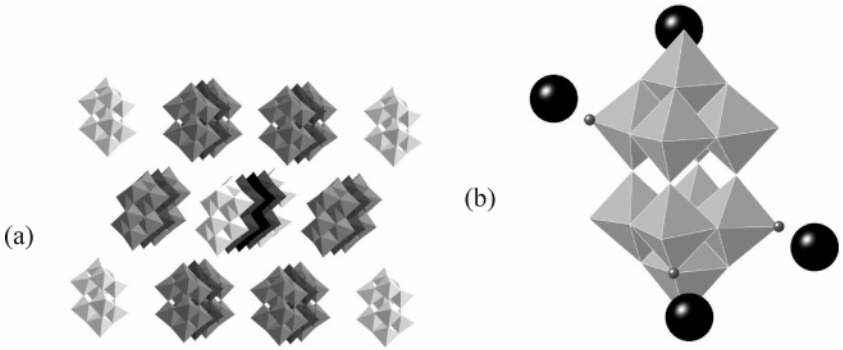

Figure 3. Embedding of punctual charges and TIPs. (a) Decawolframate anions considered in the embedding. At increasing distances, one can see a hexagonal bipyramid (dark), a hexagonal prism (lighter) and an octahedron (lightest). (b) Position of the four countercations relative to each decawolframate anion. The position of the nitrogens is shown, as are the nearest oxo ligands: O_{14}^{br} and O_5^{ap}.

TABLE 1: Comparisons of the *t*, *J*, ϵ, and *V* Parameters Extracted at the CASCI Level on Some Dimers or Trimers with One or Two 'Extra' Electrons[a]

meV	1e−/2W	2e−/2W	1e−/3W	2e−/3W
t_{13}	−410		−429/−426	−315/−325
t_{14}	−428		−453/−451	−354/−346
J_{13}		−44		−50/−28
J_{14}		−44		−52/−72
$\epsilon_3 - \epsilon_1$	−1275		−1235/−1445	
$\epsilon_4 - \epsilon_1$	−1200		−1216/−1411	
$V_{14} - V_{13}$		*		-70 ± 200

[a] Value * was not directly extracted, but supposed negligible during the extraction of the *V* parameters. Indeed, the estimation of $V_{14} - V_{13}$ (-70 ± 200 meV) is under the range of error.

TABLE 2: Comparisons of the *t*, *J*, and ϵ Parameters (in meV) Extracted at the CASCI and DDCI Level of Calculations on Some Dimers

meV	CASCI	DDCI
t_{13}	−410	−364
t_{14}	−428	−397
J_{13}	−43	−122
J_{14}	−44	−133
$\epsilon_3 - \epsilon_1$	−1275	−1272
$\epsilon_4 - \epsilon_1$	−1200	−1186

TABLE 3: Values (Calculated at the DDCI Level) of *t* and *J* vs Angles W−O−W for All Dimers of Types a, b, and c, as Well as Averages for Each Class

fragment	*t* (meV)	*J* (meV)	W−O−W (deg)
1−2	−427	−156	115.6
1−3	−364	−122	114.9
1−4	−397	−133	114.3
1−5	−347	−94	112.3
a	−384	−123	114.3
2−3	−556	−260	117.3
3−4	−542	−241	116.0
4−5	−561	−268	117.8
2−5	−515	−232	118.6
b	−544	−250	117.4
2−4′	−719	−432	173.2
3−5′	−672	−391	177.3
c	−696	−411	175.3

and −700 meV in $t_{\mathbf{c}}$. The negative sign is coherent with the results obtained on the Keggin anion.

The main result about orbital energies is the singularity of the apical cations, where a higher orbital energy is predicted, about 1 eV. The slight differences between the four equatorial wolframs are within the error range of our calculations.

Concerning Coulombic repulsion energies, as we are interested in comparing the energies of different electronic distributions, rather than in absolute repulsion values, the lowest repulsion is taken as the reference. The values for every possible W−W pair is taken into account, although they are grouped into classes following Figure 2. It can be seen that they almost follow the inverse order of average intersite distance.

TABLE 4: Values of Orbital Energy ϵ; ϵ_1 Is Taken as the Reference

$\epsilon_2 - \epsilon_1$ (meV)	$\epsilon_3 - \epsilon_1$ (meV)	$\epsilon_4 - \epsilon_1$ (meV)	$\epsilon_5 - \epsilon_1$ (meV)
−1140	−1200	−1180	−1020

TABLE 5: Values of the Intersite Electrostatic Repulsion *V* from SCF Calculations and of the Average Intersite Distance *d* for Each Dimer Type[a]

type	*V* (meV)	*d* (Å)
a, **b**	2100	3.3
c	2400	3.8
d	1250	4.6
e	1300	5.0
f	1000	6.0
g	650	6.6
h	0	8.5

[a] As indicated in the text, the lowest repulsion, *V*(*h*), is taken as arbitrary reference.

Magnetostructural Correlations in Fragments. Table 3 shows some magnetostructural data. There is a clear negative correlation with W−O−W angle for both *J* and *t*. Figure 4 shows that the correlation is fairly linear for edge-sharing fragments (type **a** and **b**). Fragment 3−4 (116°), the one where the oxygens in the coordination sphere are farthest to the countercations, is the main divergence from linearity. As expected, there is an intensification of magnetic exchange and electron transfer with increasing W−O−W angle. A similar result was obtained for the Keggin anion.[10a]

In Figure 5, we can see the calculated electrostatic repulsion compared to the curve one would get from punctual charges in vacuum estimation. As from the ab initio calculations, we can only extract differences in repulsions, and we choose the fragment with the longest distance as energy origin for both ab initio and punctual charge evaluations. That way, deviations over the continuous line means a larger shielding, while deviations under it means smaller shielding. Overall, one can see that the trivial punctual charge estimation would have been fairly good.

Electronic and Magnetic Structure of the Anion. In this section, we present the results of model Hamiltonian calculations involving one and two delocalized "extra" electrons over the 10 d-orbitals of decawolframate. We consider two observables: the distribution of the "extra" electrons between equatorial and apical WO_6 sites, and the singlet-to-triplet energy gap (for two "extra" electrons).

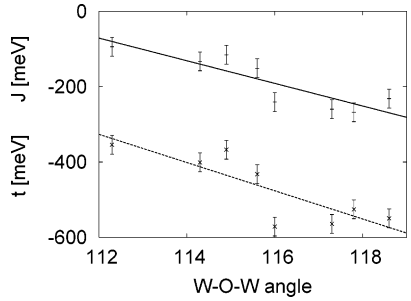

Figure 4. Magnetostructural correlations for type **a** and type **b** fragments. Full lines: calculated magnetic exchange J vs W−O−W angle. Dashed lines: calculated electron transfer t vs W−O−W angle. Values at the DDCI level.

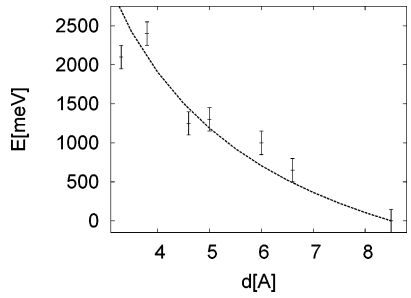

Figure 5. Calculated electrostatic repulsion vs W−W distance: ab initio values as points with error bars, punctual charges in vacuum as line.

By using the parameters of Tables 3, 4, and 5, we predict for the ground state of the one-electron reduced system that a 95% of the electronic density is on the eight equatorial sites and 5% on the two apical sites, far from the 80%/20% homogeneous distribution. This deficit was expected, as the orbital energies differences favor the occupation of the equatorial sites.

For the two-electron situation, it is predicted that 91% of the electronic density is onto the eight equatorial sites and 9% onto the two apical ones. It is also shown that almost all the population of the apical center originates from distributions with one electron on an apical center and one electron on an equatorial (the contribution to the apical density of the situation with one electron on each W(1) apical center is almost zero). This shows that even though the electrostatic repulsion favors the increase of the interelectronic distance, it is not strong enough to compensate the electronic "deficit" of the apical wolfram atoms. The singlet-to-triplet energy gap is evaluated to 780 meV and explains the diamagnetism of the two-electron reduced decawolframate polyanion. This quite large energy gap is of the same order of magnitude as the ones found in other dirreduced polyoxometalates, like the Keggin anion.[10]

The antagonistic roles of the various microscopic parameters (t, J, ϵ, and V) acting in the two-electron reduced system motivate a deeper analysis of their influence. With this goal, the variations of the observables of the whole two-electron reduced decawolframate versus the variations of the microscopic parameters are plotted.

Interplay between Parameters: Competition between Electrostatic Repulsion and Orbital Energy. The most evident effect to expect is the competition between electrostatic repulsion, which tends to stabilize a maximum separation of the electrons on the two apical W(1) atoms and orbital energy, which favors the population of the equatorial sites (because ϵ_1 is almost 1 eV higher than ϵ_{2-5}). One can also anticipate that the electronic distribution has a dramatic effect on the electronic interactions and thus on the magnetic coupling; the spins will uncouple if they get strongly localized in very distant centers.

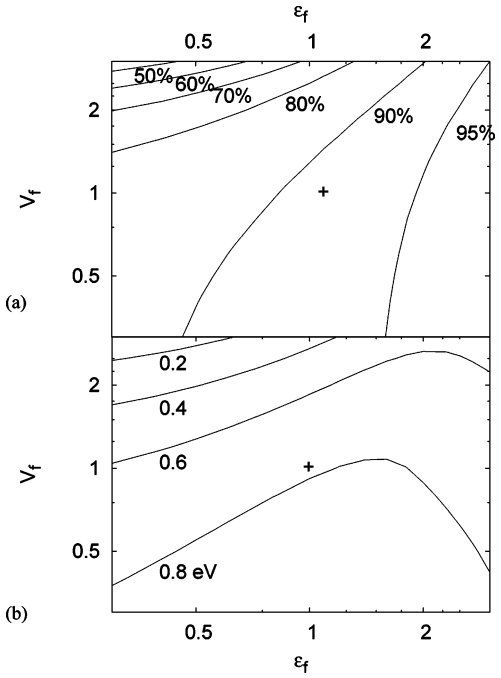

Figure 6. Variations of (a) the electron density of the equatorial sites and (b) the singlet−triplet energy gap with factors multiplying all Coulombic repulsions (V_f) and all orbital energies (ϵ_f). Note that the coordinates are logarithmical.

To confirm these predictions, and to check the influence of an over- or underestimation of orbital and electrostatic repulsion energies, we display in Figure 6 the changes of the observables on a wide range of V, ϵ, multiplying the ab initio values by factors ranging from $^1/_3$ to 3. As expected, orbital energy and electrostatic repulsion play an antagonistic role on the electronic distribution. In simple terms, the higher the difference in electrostatic repulsion, the higher the probability of finding the electrons on the apical metals, while the higher the differences in orbital energies, the higher the probability to find them in the equatorials. As can be seen, a population distribution higher than the homogeneous 80/20 is predicted even if we assume an overestimation of 50% in ϵ differences and an underestimation of 50% in V differences.

Bond-distance studies[20] and NMR of ^{183}W, ^{31}P, and ^{17}O[7] indicate a strong apex-equator asymmetry of the electron distribution. Vibronic calculations[16] predict that the electron population on apical centers is negligible. Our calculations basically confirm and rationalize the experimental results, but we do predict a non-negligible electron density in apical sites. In this regard our ab initio predictions agree with those of the DFT approach (cf. the data in the tables of reference[17]). This apparent overestimation of the apical population might be due to the omission of the vibronic coupling into the calculations that could play a role in the electronic distribution.

The next logical step is to analyze the effects on the magnetic properties. A certain but not dramatic influence of electrostatic repulsion on the singlet-to-triplet energy gap was found, namely the gap increases for lower values of V and decreases for high values of V. This is an expected trend, as a large interelectronic distance should impair the antiferromagnetic interaction. It is more interesting to note the influence of the orbital energies ϵ. One observes that, up to a certain point, larger orbital energy differences favor the interaction because it shifts the electrons from the apical to the equatorial sites. If too large, however, the electrons might be "trapped" into the most stable equatorial

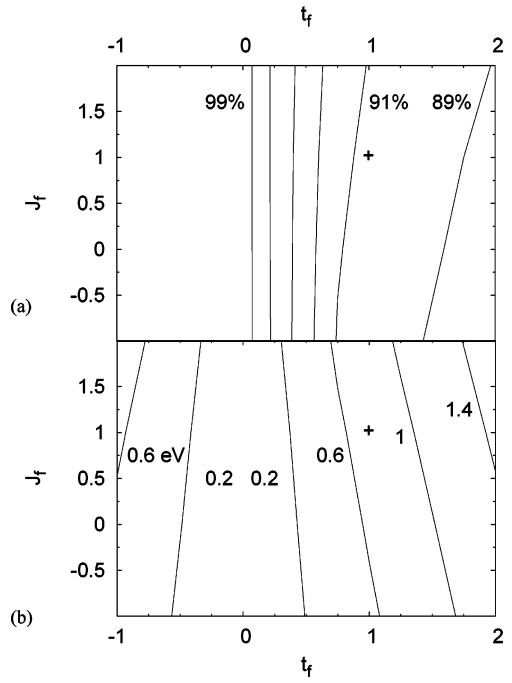

Figure 7. Variation of (a) the electron density of the equatorial sites and (b) the singlet-to-triplet energy gap with factors multiplying all magnetic exchange parameters (J_f) and all electron transfers (t_f). One can see the leading role of t.

metals, on opposite, far positions (Figure 2 **f**, 6 Å), thus diminishing the singlet-to-triplet energy gap.

Interplay between Parameters: Magnetic Exchange and Electron Transfer. Yamase,[20] among others, postulated that the electron transfer is weak for edge-sharing octahedra, as seen in the weak delocalization of the unpaired electron in monoreduced W_6O_{19}.[21] Delocalization goes on mainly through quasi-linear W−O−W bonds. Thus, diamagnetism in direduced decawolframate should be attributed to a strong antiferromagnetic exchange mediated by intersquare transfer. Our calculations show that, even if the hopping increases with the linearity of the W−O−W angle, the other transfer pathways (specially intrasquare) are very important, while magnetic exchange is far from being a critical interaction in the final magnetic behavior of the system.

As shown in Figure 7, electron transfer has a dramatic influence both in the electronic distribution and in the magnetic properties of the system. A change of the sign of all the t parameters annihilates the electronic population of the apical centers. The singlet-to-triplet energy gap, while not so heavily dependent on the sign, is nearly proportional to the value of the transfer parameter. The gap is remarkably symmetrical regarding t, at least when all transfer parameters are simultaneously raised or lowered.

The influence of J, in contrast, is very limited (and evidently does not display sign-symmetry). For a given t, a much higher antiferromagnetic J results in a slightly larger energy gap. Moreover, even if the antiferromagnetic exchange is canceled, or replaced with a strong ferromagnetic exchange, the singlet remains well below the triplet. The influence on the electronic distribution is also very weak.

If communication through both t_c and J_c between the squares is canceled, the singlet-to-triplet gap disappears, as the electrons have no way to interact. Moreover, if we just eliminate the intersquare t_c, the gap closes considerably, the only remaining coupling mechanism being a combination of intrasquare t_b + intersquare J_c.

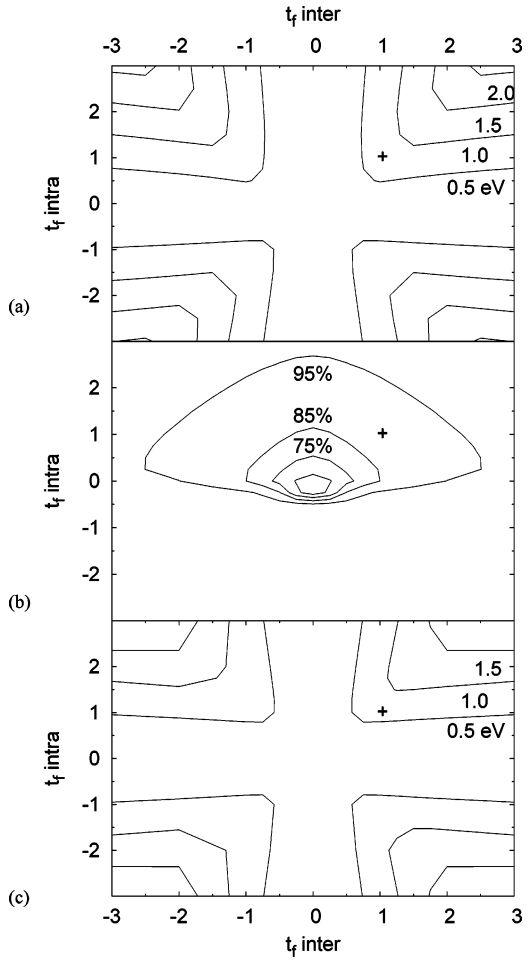

Figure 8. Variation of the singlet-to-triplet energy gap (a), of the electron density of the equatorial sites (b), and variation of the same energy gap when transfer with apical wolfram is not allowed (c). The axes indicate the factor multiplying all ab initio values of intrapyramid transfer t_b and interpyramid transfer t_c.

Interplay between Parameters: Role of the Different Transfer Pathways. The influence of the relative intensity of the intra- and intersquare electron-transfer processes is drawn in Figure 8. It can be seen that for the energy gap as well as for the electronic distribution, the near-symmetry of Figure 7b is lifted for intrasquare transfer, while for the intersquare transfer, it becomes strict. The system is also strictly symmetric, both in electronic distribution and in energy, with the sign of apical−square transfer t_a (data not shown).

The gap is maximized when the two hopping parameters are high (in absolute value). When either of them is low, or in general, when the ratio t_i/t_j is very different from unity, the gap drops.

The calculations were repeated for an artificially high value of repulsion V for nearest neighbors (not shown in graphics). The gap diminished to about 50%, but the general form of the surfaces was not altered. Hence, we see that nearest-neighbor repulsions are important, but not dramatic, for the general magnetic behavior. The calculations were also repeated, cancelling the apical−square transfer t_a (Figure 8c). Both the general form of the surface and the magnitude of the gap were maintained, but now the sign-symmetry is strict for both remaining hopping parameters.

It is interesting to revisit reference 16a. With our current results in mind, we confirm their hypothesis of the negative sign of t, however, we obtain a different ordering in the absolute

values. It would be of great interest, in our thinking, to repeat the vibronic study now that we have provided ab initio quality values for t, ϵ, V, and J.

Conclusions

In this work we have established the origin of the strong spin interaction between the two delocalized electrons present in the reduced polyoxometalate $W_{10}O_{32}^{6-}$. We predict a singlet−triplet energy gap of 780 meV ($\simeq$6000 cm^{-1}) and 91% of the electronic population on the square WO_6 octahedra. Thus, the diamagnetism in this POM mainly arises from the delocalization of the two "blue" electrons over the two central W_4O_{16} squares. Each one of the two electrons is circulating over one of the two squares to minimize electron repulsion, and the strong antiferromagnetic coupling between them is dominated by the two (intrasquare and intersquare) hopping integrals.

Interestingly, the exchange interaction J only plays a minor role, while the electron-transfer governs both the singlet−triplet energy gap and the electronic distribution. In fact, the $S = 0$ ground spin state is independent of the sign of J and is stabilized even in the presence of strong ferromagnetic exchange. On the other hand, it has been found that the "blue" electrons are mainly distributed on the two central W_4O_{16} squares, the two apical centers having an electron density below a half of the value expected for a homogeneous charge distribution.

These conclusions have been extracted from a model that considers a phenomenological Hamiltonian that takes into account the main electronic parameters: electron transfer (t), magnetic exchange (J), relative electrostatic repulsions (V), and orbital energies (ϵ) with an ab initio evaluation of these parameters. This example constitutes the most complex POM system for which this methodology has been successfully applied so far. In fact, we have determined up to 48 independent parameters (10J, 10t, 24V, 4ϵ) from first principles, compared with the previous case, the Keggin anion, which included nine independent parameters (3J, 3t, 3V).

The size of the system has permitted introducing all of these parameters into the model Hamiltonian. This feature has provided the opportunity to study in detail the effect of each one of the parameters in the magnetic and electronic structure of this high-nuclearity mixed-valence cluster.

Acknowledgment. This work has been performed in the framework of the NoE MAGMANet and the D26 COST action "Understanding and predicting the electronic, magnetic, and structural properties of polyoxometalates". We thank Alain Gellé for his Boys localization program, Carmen Jiménez-Calzado for her effective Hamiltonian extraction program and Marie-Bernadette Lepetit, Nathalie Guihéry, and Jean-Paul Malrieu for fruitful discussions. We thank the computational center IDRIS/CNRS (Paris) where the calculations were performed under project no. 1104 and the computational center of the University of Valencia. The spanish MEC is acknowledged for financial support (grants CTQ2005-09385-C03-01 and MAT2004-03849). The Generalitat Valenciana is acknowledged for financial support and for a predoctoral grant and a postdoctoral contract to A. Gaita-Ariño. The work in France has been supported by the CNRS and the UPS.

Appendix: Computational and Modeling Details

The CASSCF procedure permits a very accurate treatment of the polarization and correlation of the "extra" electrons (captured during the oxido−reduction processes) in the *mean field* of the other (closed-shell) electrons. The results (energies, wave functions, and molecular orbitals) provide a good zeroth order for treating the dynamical polarization and correlation effects. This can be done variationally with the difference dedicated configuration interaction (DDCI) methods. The DDCI matrix is based on the configurations that provide the main *differential* contributions to the lowest states. Hence, DDCI calculations provide a very accurate evaluation of the microscopic parameters relevant for magnetic compounds but do not permit to extract informations about *absolute energies* but about *energy differences* (and wave functions). The DDCI method is now quietly widely used, and more details can be found for exemple in references.[10] CASSCF is part of the MOLCAS suite of programs,[22] and the DDCI results are obtained with the CASDI code.[23]

TABLE 6: Representative Matrix of the Model Hamiltonian Restricted to the Case of One Electron Delocalized between Two Orbitals *a* and *b*

	$\|a\rangle$	$\|b\rangle$
$\|a\rangle$	0	t_{ab}
$\|b\rangle$	t_{ab}	$\epsilon_b - \epsilon_a$

In all the calculations, the inner-core electrons ([$1s^2 2s^2 2p^6 3s^2 3p^6 4s^2 3d^{10} 4p^6 5s^2 4d^{10} 4f^{14}$] for the W atoms and [$1s^2$] for the O atoms) are represented by effective core potentials (ECP). The outer-core and valence electrons are represented using a 13s10p9d5f primitive basis set contracted to 3s3p4d2f for the W, a 5s6p1d primitive basis set contracted to 1s2p1d for the apical O atoms, and a 5s6p1d primitive basis set contracted to 2s4p1d for the other O. Exact expressions of the basis sets and ECP can be found in ref 24.

Model Hamitonians on Embedded Fragments. The evaluation of the microscopic parameters of such a Hamiltonian from ab initio calculations is a crucial point. We have now some experience in the evaluation of the magnetic exchange integral and of the electron transfer integral between crystallographically equivalent centers (it was widely detailed in the case of a T_d Keggin anion where all the W centers are crystallographically equivalent[10]). Still, the complete evaluation of the microscopic parameters is much harder in the present case due to the complexity of the model Hamiltonian and to the low symmetry of the compound.

For each fragment, two kinds of calculations were performed. Calculations involving one "extra" electron (above the closed-shell electrons) permit an evaluation of ϵ (the orbital energy) and t (electron transfer), and calculations with two "extra" electrons permit an evaluation of J (magnetic exchange) and V (intersite electrostatic repulsion).

Electron Transfer and Orbital Energy. The representative matrix of the model Hamiltonian restricted to the case of one electron delocalized between two orbitals a and b is given by matrix of Table 6, where $|a\rangle$ (respectively $|b\rangle$) is the Slater determinant representing an "extra" electron in orbital a (respectively b). As the absolute orbital energy is meaningless in the model, the difference $\epsilon_a - \epsilon_b$ suffices for our considerations, and we choose ϵ_a as energy reference.

The eigenvalues and the coefficients onto $|a\rangle$ and $|b\rangle$ (this set of determinants defines the model space) of the doublet eigenstates obtained from ab initio calculations are used in an effective Hamiltonian extraction procedure. The effective Hamiltonian H_{eff} has a similar form as the model Hamiltonian and verifies the equation: where E_i are the ab initio energies

$$H_{\text{eff}}\,\Psi_i^{\text{proj}} = E_{\text{i}}\Psi_i^{\text{proj}} \qquad (1)$$

and Ψ_i^{proj} are the corresponding ab initio wave functions projected onto the model space. This procedure permits a direct

TABLE 7: Representative Matrix of the Model Hamiltonian Restricted to the Case of Two Electrons Delocalized between Two Orbitals *a* and *b*

	$\|a\bar{b}\rangle$	$\|\bar{a}b\rangle$	$\|a\bar{a}\rangle$	$\|b\bar{b}\rangle$
$\|a\bar{b}\rangle$	0	0	t_{ab}	t_{ab}
$\|\bar{a}b\rangle$	0	0	$-t_{ab}$	$-t_{ab}$
$\|a\bar{a}\rangle$	t_{ab}	$-t_{ab}$	$U_a - V_{ab} + \epsilon_a - \epsilon_b$	0
$\|b\bar{b}\rangle$	t_{ab}	$-t_{ab}$	0	$U_b - V_{ab} - \epsilon_a + \epsilon_b$

evaluation of the parameters of the model Hamiltonian (the energy difference between the two ϵ orbital and the t transfer integral between them). As the projections of the ab initio wave functions do not have any reason to be orthogonal, the effective Hamiltonian is not necesseraly hermitic, providing two different values for the same t parameter. Nevertheless, whatever the fragment and the level of calculation, the wave functions have a large weight onto the model space (more than 80%) and the effective Hamiltonian is almost hermitic. Thus, the value given in the results section do not indicate this slight nonhermiticity. More details on effective Hamiltonians can be found in ref 25.

Two sets of molecular orbitals (MO) were used for DDCI calculations: CASSCF orbitals of the triplet state (obtained with 2 "extra" electrons) and IDDCI1 orbitals for the two lowest doublet states. IDDCI1 (or IMONO) MO are adapted to the calculations of energy differences. The MO are the average natural orbitals obtained from iterative calculations at the IC+MONO level of the two lowest doublet states that take into account the dynamical polarization of the two d_{xy}-like orbitals. As it is usually observed, the t parameter is not very sensitive to the set of MO (changes are of the order of 5%). We also checked that energy orbital values ϵ are almost independent of the choice of CASSCF or IDDCI1 MO (changes are of the order of 2%). These results are not reported in this work.

Finally, in order to extract the model Hamiltonian parameters from ab initio calculations, a localization of the MO was done following the Boys criteria.[26] We obtained two orthogonal MO, one almost localized on one metal center (named *a*) and the other almost localized on the other metal center (named *b*).[27]

A similar procedure is used to extract ϵ and t parameters from trimer fragments containing one "extra" electron. The model and effective Hamiltonians are 3×3 matrices, permitting the simultaneous evaluation of the three ϵ orbital energies and the three t transfer integrals.

Intersite Electrostatic Repulsion and Magnetic Exchange. Calculations on dimer fragments containing two "extra" electrons permit one to evaluate the magnetic exchange (J) and intersite electrostatic repulsion (V) parameters between the pairs of W centers contained in the considered dimer fragment.

The extraction of J is simply obtained by the energy difference between the singlet state essentially based on the configuration $(|a\bar{b}\rangle - |\bar{a}b\rangle)/\sqrt{2}$ and the triplet state essentially based on $(|a\bar{b}\rangle + |\bar{a}b\rangle)/\sqrt{2}$:

$$J = E_S - E_T \tag{2}$$

where E_S is the energy of the singlet state and E_T the energy of the triplet state ($J > 0$ is ferromagnetic).

The evaluation of V is more complicated, as it demands one to compare energies of states with different occupation of the magnetic d orbital of the W centers. We have to consider four determinants ($|a\bar{b}\rangle$, $|\bar{a}b\rangle$, $|a\bar{a}\rangle$, and $|b\bar{b}\rangle$) and their interaction, representated in the matrix given in Table 7, where the energy of the determinants $|a\bar{b}\rangle$ or $|\bar{a}b\rangle$ is chosen as the reference, U_a (respectively U_b) is the intrasite electrostatic repulsion of two electrons in orbital *a* (respectively *b*), V_{ab} the intersite electrostatic repulsion of two electrons in orbitals *a* and *b* and t_{ab} the electron transfer between orbitals *a* and *b*.

TABLE 8: Representative Matrix of the Model Hamiltonian of Two Electrons Delocalized between Three Orbitals *a*, *b*, and *c*[a]

	$\|a\bar{b}\rangle$	$\|\bar{a}b\rangle$	$\|a\bar{c}\rangle$	$\|\bar{a}c\rangle$	$\|b\bar{c}\rangle$	$\|\bar{b}c\rangle$
$\|a\bar{b}\rangle$	E_{ab}	$J_{ab}/2$	t_{bc}	e_a	e_b	$-t_{ac}$
$\|\bar{a}b\rangle$	$J_{ab}/2$	E_{ab}	e_a	t_{bc}	$-t_{ac}$	e_b
$\|a\bar{c}\rangle$	t_{bc}	e_a	E_{ac}	$J_{ac}/2$	t_{ab}	e_b
$\|\bar{a}c\rangle$	e_a	t_{bc}	$J_{ac}/2$	E_{ac}	e_c	t_{ab}
$\|b\bar{c}\rangle$	e_b	$-t_{ac}$	t_{ab}	e_c	E_{bc}	$J_{bc}/2$
$\|\bar{b}c\rangle$	$-t_{ac}$	e_b	e_c	t_{ab}	$J_{bc}/2$	E_{bc}

[a] e parameters stand for exchange transfers interaction ($e_a = \langle a\bar{b}|H|\bar{a}c\rangle$, for example) are neglected. E_{ab}, E_{ac}, and E_{bc} stand for $V_{ab} + \epsilon_a + \epsilon_b$, $V_{ac} + \epsilon_a + \epsilon_c$, and $V_{bc} + \epsilon_b + \epsilon_c$, respectively.

The evaluation of the E_{aa} and E_{bb} energies of the $|a\bar{a}\rangle$ and $|b\bar{b}\rangle$ determinants was done following an idea of Malrieu.[28] A set of molecular orbitals is obtained at the CASSCF level of calculation for the $(|a\bar{b}\rangle + |\bar{a}b\rangle)/\sqrt{2}$ triplet state. Then, a Boys localization procedure[26,27] gives two orthogonal MO, one almost localized on one metal center (named *a*) and the other almost localized on the other metal center (named *b*). Then, a SCF procedure is performed to reoptimize all the orbitals except *b* (respectively *a*) with two electrons in *a* (respectively *b*) and zero in *b* (respectively *a*). For fragments based on distant enough W, the electron transfer t being almost 0, the matrix (Table 7) is almost diagonal. Then, one of the two first singlet excited states is almost $|a\bar{a}\rangle$ (energy $U_a - V_{ab} + \epsilon_a - \epsilon_b$) and the other is almost $|b\bar{b}\rangle$ (energy $U_b - V_{ab} - \epsilon_a + \epsilon_b$). The advantage of this procedure is that it only necessitates two SCF calculations, while DDCI calculations would have to diagonalize a matrix of tens of millions of determinants.

Calculations on trimer fragments containing two "extra" electrons are very interesting to evaluate V (Table 8 represents the corresponding model Hamiltonian). Indeed, the evaluation can be done by considering only determinants with zero or one electron in the magnetic local orbitals, whereas determinants with two electrons in the same local orbital (with a very high energy) have also to be considered in dimer fragments with two "extra" electrons.

Three singlet and three triplet states are calculated at the CASCI level on the CASSCF orbitals optimized for the three triplet states. The corresponding energies and wave functions permit, through an effective Hamiltonian procedure, to evaluate all the paramaters of matrix 8. Therefore, trimer calculations with two "extra" electrons provide also an evaluation of the superexchange (J) and exchange transfer (e, see ref 10c) parameters. Finally, an evaluation of the influence of the presence of an "extra" electron on the transfer of another "extra" electron can be obtained by comparing the t evaluation from trimer calculations with one or two "extra" electrons.

More sophisticated calculations (DDCI) would be interesting to evaluate regarding the influence of dynamical mechanisms. However, these calculations would be very large, and an alternative procedure (equivalent to that for V evaluation from dimer calculations) is used. Average orbitals for the three triplet states generated by two electrons delocalized over the three centers is obtained at the CASSCF level. Then, one of the three active orbitals is frozen and reoptimization of the two remaining active orbitals is performed at the CASSCF level for the triplet state. This permits one to evaluate of the energy of $|ab\rangle$, $|ac\rangle$, and $|bc\rangle$ determinants and to compare their energies. More details about this "constrained CASSCF" method and compari-

sons with DDCI results on various type of compounds will be published in a forthcoming article.

References and Notes

(1) de Luyart Lubice, J. J.; de Luyart Lubice, F. D. *Extractos Juntas Generales R. Soc. Basc.* **1783**, 46−88; Berzelius, J. *Pogg. Annu.* **1826**, *6*, 369; Keggin, J. F. *Nature* **1933**, *131*, 908.

(2) (a) Pope, M. T. *Isopoly and Heteropoly Metalates*; Springer-Verlag: Berlin, 1983. (b) Pope, M. T.; Müller, A. *Polyoxometalates: From Platonic Solids to Antiretroviral Activity*; Kluwer Academic: Dordrecht, The Netherlands, 1994. (c) *Chem. Rev.* **1998**, *98*. (d) Pope, M. T.; Müller, A. *Polyoxometalate Chemistry From Topology via Self-Assembly to Applications*; Kluwer Academic: Dordrecht, The Netherlands, 2001. (e) Yamase, T.; Pope, M. T. *Polyoxometalate Chemistry for Nanocomposite Design*, Kluwer Academic/Plenum Publishers: New York, 2002. (f) Borrás-Almenar, J. J.; Coronado, E.; Müller, A.; Pope, M. T. *Polyoxometalate Molecular Science*; Kluwer Academic: Dordrecht, The Netherlands, 2003.

(3) (a) Borrás-Almenar, J. J.; Clemente-Juan, J. M.; Coronado, E.; Palii, A. V.; Tsukerblat, B. S. *J. Chem. Phys.* **1996**, *105*, 6892−6909. (b) Borrás-Almenar, J. J.; Clemente-Juan, J. M.; Coronado, E.; Tsukerblat, B. S. *Inorg. Chem.* **1999**, *38*, 6081−6088.

(4) Müller, A.; Luban, M.; Schröder, C.; Modler, R.; Kögerler, P.; Axenovich, M.; Schnack, J.; Canfield, P.; Budk'ko, S.; Harrison, N. *ChemPhysChem* **2001**, *2*, 517−521.

(5) (a) Handrick, K.; Malrieu, J. P.; Castell, O. *J. Chem. Phys.* **1994**, *101*, 2205−2212. (b) Calzado, C. J.; Cabrero, J.; Malrieu, J. P.; Caballol, R. *J. Chem. Phys.* **2002**, *116*, 2728.

(6) (a) Pope, M. T.; Varga, G. M. *Inorg. Chem.* **1966**, *5*, 1249−1254; (b) Pope, M. T.; Papaconstantininou, E. *Inorg. Chem.* **1977**, *6*, 1147−1152; (c) Papaconstantininou, E.; Pope, M. T. *Inorg. Chem.* **1977**, *6*, 1152−1155; (d) Varga, G. M.; Papaconstantininou, E.; Pope, M. T. *Inorg. Chem.* **1970**, *9*, 662−667 (e) Papaconstantininou, E.; Pope, M. T. *Inorg. Chem.* **1970**, *9*, 667−669.

(7) Kazansky, L. P.; McGarvey, B. R. *Coord. Chem. Rev.* **1999**, *188*, 157−210.

(8) (a) Borrás-Almenar, J. J.; Clemente-Juan, J. M.; Coronado, E.; Tsukerblat, B. S. *Chem. Phys.* **1995**, *195*, 1−15. (b) Borrás-Almenar, J. J.; Clemente-Juan, J. M.; Coronado, E.; Tsukerblat, B. S. *Chem. Phys.* **1995**, *195*, 17−28.

(9) Poblet, J. M.; López, X.; Bo, C. *Chem. Soc. Rev.* **2003**, 297−308.

(10) (a) Suaud, N.; Gaita-Ariño, A.; Clemente-Juan, J. M.; Sánchez-Marín, J.; Coronado, E. *J. Am. Chem. Soc.* **2002**, *124*, 15134. (b) Suaud, N.; Gaita-Ariño, A.; Clemente-Juan, J. M.; Sánchez-Marín, J.; Coronado, E. *Polyhedron* **2003**, *22* (14−17), 2331−2337. (c) Suaud, N.; Gaita-Ariño, A.; Clemente-Juan, J. M.; Coronado, E. *Chem.*−*Eur. J.* **2004**, *10*, 4041−4053.

(11) Fuchs, J.; Hartl, H.; Schiller, W.; Gerlach, U. *Acta Crystallogr., Sect. B: Struct. Sci.* **1976**, *32*, 740−749.

(12) (a) Tanielian, C.; Seghrouchni, R.; Schweitzer, C. *J. Phys. Chem. A* **2003**, *107*, 1102−1011. (b) Dondi, D.; Fagnoni, M.; Molinari, A.; Maldotti, A.; Albini, A. *Chem.*−*Eur. J.* **2004**, *10*, 142−148.

(13) Texier, I.; Giannotti, C.; Malato, S.; Richter, C.; Delaire, J. *Catal. Today* **1999**, *54*, 2, 11, 297−307.

(14) (a) Tanielian, C.; Schweitzer, C.; Seghrouchni, R.; Esch, M.; Mechin, R. *Photochem. Photobiol. Sci.* **2003**, *2*, 297−305. (b) Bonchio, M.; Carraro, M.; Conte, V.; Scorrano, G. *Eur. J. Org. Chem.* **2005**, 4897−4903. (c) Bonchio, M.; Carraro, M.; Scorrano, G.; Fontanova, E.; Drioli, E. *Adv. Synth. Catal.* **2003**, 1119−1126.

(15) (a) Chemseddine, A.; Sanchez, C.; Livage, J.; Launay, J. P.; Fournier, M. *Inorg. Chem.* **1984**, *23*, 2609. (b) Duncan, D. C.; Hill, C. L. *Inorg. Chem.* **1996**, *35*, 5828. (c) Lykakis, I. N.; Orfanopoulos, M. *Tetrahedron Lett.* **2005**, *46*, 7835−7839.

(16) (a) Duclusaud, H.; Borshch, S. A. *Chem. Phys. Lett.* **1998**, *290*, 526. (b) Borshch, S. A. *Inorg. Chem.* **1998**, *38*, 3116. (c) Gracia, J.; Poblet, J. M.; Fernandez, J. A.; Autschbach, J.; Kazansky, L. P. *Eur. J. Inorg. Chem.* **2006**, 1149−1154.

(17) Bridgeman, A. J.; Cavigliasso, G. *J. Phys. Chem. A* **2002**, *106*, 6114−6120.

(18) Sasaki, Y.; Yamase, T.; Ohashi, Y.; Sasada, Y. *Bull. Chem. Soc. Jpn.* **1987**, *60*, 4285−4290.

(19) (a) Suaud, N.; Lepetit, M. B. *Phys. Rev. B* **2000**, *62*, 402−409. (b) Lepetit, M.-B.; Suaud, N.; Gellé, A.; Robert, V. *J. Chem. Phys.* **2003**, *118*, 3966.

(20) Yamase, T. *J. Chem. Soc., Dalton Trans.* **1997**, 1597−1604.

(21) Sanchez, C.; Livage, J.; Launay, J. P.; Fourier, M. *J. Am. Chem. Soc.* **1993**, *105*, 6817−6823.

(22) Andersson, K.; Barysz, M.; Bernhardsson, A.; Blomberg, M. R. A.; Carissan, Y.; Cooper, D. L.; Cossi, M.; Fleig, T.; Fülscher, M. P.; Gagliardi, L.; de Graaf, C.; Hess, B. A.; Karlström, G.; Lindh, R.; Malmqvist, P.-Å.; Neogrády, P.; Olsen, J.; Roos, B. O.; Schimmelpfennig, B.; Schütz, M.; Seijo, L.; Serrano-Andrés, L.; Siegbahn, P. E. M.; Stålring, J.; Thorsteinsson, T.; Veryazov, V.; Wierzbowska, M.; Widmark, P.-O. *MOLCAS*, version 5.2; Lund University: Lund, Sweden, 2001.

(23) (a) Maynau, D.; Ben Amor, N.; Pitarch-Ruiz, J. V. *CASDI suite of programs*; University of Toulouse: Toulouse, France, 1999. (b) Ben Amor, N.; Maynau, D. *Chem. Phys. Lett.* **1998**, *286*, 211. (c) Pitarch-Ruiz, J. V.; Sánchez-Marín, J.; Maynau, D. *J. Comput. Chem.* **2002**, *23*, 1157.

(24) Barandiarán, Z.; Seijo, L. *Can. J. Chem.* **1992**, *70*, 409.

(25) (a) Bloch, C. *Nucl. Phys.* **1958**, *6*, 329. (b) des Cloizeaux, J. *Nucl. Phys.* **1960**, *20*, 321.

(26) (a) Boys, S. F. *Rev. Mod. Phys.* **1960**, *32*, 296. (b) Foster, J. M.; Boys, S. F. *Rev. Mod. Phys.* **1960**, *32*, 300.

(27) The calculation was performed using a program developed by Alain Gellé. Ph.D. Thesis, Université Paul Sabatier, Toulouse, France, 2004.

(28) Malrieu, J.-P.; IRSAMC, Université Paul Sabatier, Toulouse, France; Private communication, 2005.

(29) Calzado, C.; Malrieu, J.-P. *Phys. Rev. B* **2001**, *63*, 214520.